PROCEEDINGS OF SCIENCE

Data reconstruction and classification with graph neural networks in KM3NeT/ARCA6-8

Francesco Filippini,[a,b,*] **Eleni Androutsou,**[c] **Alba Domi,**[d] **Bernardino Spisso,**[e,f,g] **and Evangelia Drakopoulou**[c] **on behalf of the KM3NeT collaboration**

[a] *Università di Bologna, Dipartimento di Fisica e Astronomia, v.le C. Berti-Pichat, 6/2, Bologna, 40127, Italy*

[b] *INFN, Sezione di Bologna, v.le C. Berti-Pichat, 6/2, Bologna, 40127, Italy*

[c] *NCSR Demokritos, Institute of Nuclear and Particle Physics, Ag. Paraskevi Attikis, Athens, 15310, Greece*

[d] *Erlangen Centre for Astroparticle Physics of Friedrich-Alexander-Universität, Nikolaus-Fiebiger-Straße 2, 91058 Erlangen*

[e] *INFN, Sezione di Napoli, Complesso Universitario di Monte S. Angelo, Via Cintia ed. G, Napoli, 80126, Italy*

[f] *Gruppo Collegato di Salerno, Dipartimento di Fisica, Via Giovanni Paolo II 132, Fisciano, 84084, Italy*

E-mail: francesco.filippini9@unibo.it, androutsou@inp.demokritos.gr, Alba.Domi@ge.infn.it, Spisso@na.infn.it, drakopoulou@inp.demokritos.gr

KM3NeT is a research infrastructure hosting two large-volume Cherenkov neutrino detectors which are currently under construction in the Mediterranean Sea. The KM3NeT/ARCA detector is optimised for the detection of high-energy neutrinos from astrophysical sources in the TeV-PeV energy range. Once completed, the detector will consist of 230 detection units. Here, we present a Deep Learning method using graph neural networks that is trained and applied to events gathered with 6 and 8 active detection units of KM3NeT/ARCA. Graph neural networks have been trained for classification and regression tasks, showing very promising performances in a range of different tasks like neutrino-background identification, neutrino event topology classification, energy and direction reconstruction, and also in the study of properties of muon bundles.

38th International Cosmic Ray Conference (ICRC2023)
26 July - 3 August, 2023
Nagoya, Japan

ICRC2023
38th International Cosmic Ray Conference
The Astroparticle Physics Conference

*Speaker

PoS(ICRC2023)1194

1. Introduction

Charged particles produced in neutrino interactions with water induce Cherenkov light, which is detected by 3" photomultiplier tubes (PMTs) hosted in pressure resistant glass spheres. 31 PMTs are stored in a single digital optical module (DOM), and 18 DOMs are fixed to a long vertical detection unit (DU) that is anchored to the sea floor. Each of the building blocks of KM3NeT will consist of 115 DUs [1]. The KM3NeT detector can therefore be modelled as a 3D array of photosensors capable of registering the arrival time and time over threshold of photons impinging on a photomultiplier tube (hit) contained inside a DOM. The detected light on each PMT can be used to reconstruct the particle properties, such as their energy or direction. Each hit has information about the time and the xyz-position of the PMT that recorded the light, as well as its pointing direction. All the hit information of an event serves as input to reconstruction and classification algorithms. Since data recorded by KM3NeT closely resembles point clouds, graph neural networks (GNNs) are a natural choice as architecture for deep neural networks employed for the data analysis.

2. Graph neural networks

In the past, Deep Learning methods have acquired huge popularity on image recognition tasks, exploiting convolution and pooling operations on images encoded as a fix grid of pixels. These techniques have also been developed in the context of the KM3NeT experiment [2]. However, the fixed pixel structure has shown limitations in its capability to represent data collected by the telescope. The high dimensionality and sparse signal registered in the detector can be much better encoded in graphs. Other advantages of graphs with respect to image based methods are linked to the limited resolution in position and time that can be achieved through images/fixed grid pixels. At the same time, DOMs in the KM3NeT detector move under the effect of the sea current: this information is completely lost within the position bin size. The most natural way to encode information of events into a graph is to represent every photon hit as a node. Therefore, each node has a 7-dimensional feature space represented by: 3 spatial coordinates, 3 PMT directions, and time. To create the final graph structures then, nodes are connected to each other, based on Euclidean metric. For memory usage optimization and for keeping the number of connections under control, each node is connected to its *k-nearest neighbours*. For the model architecture adopted in the next sections, the ParticleNet architecture has been exploited [3]. This architecture was originally designed for point cloud applications, and used for jet tagging at LHC, showing outstanding performances with respect to image convolutional techniques.

3. Event reconstruction and classification

3.1 Neutrino energy regression

The architecture explained in Section 2 has been exploited using a last fully-connected layer with a linear activation function in order to produce an estimation of neutrino energy. The training was performed with about 4 million simulated events of ARCA, with 6 active DUs, equally divided among track-like (ν_μ charged current interaction) and shower-like events (ν_μ neutral current, ν_e charged current, ν_e neutral current interaction), including the corresponding antiparticles. The

validation data set was composed of 200k events. The Monte Carlo (MC) simulated energy is used as truth reference value for this learning task. A r^2 score (coefficient of determination[1]) is computed on a test data set, reaching a value of 0.835. For comparison, the r^2 score achieved by the standard reconstruction algorithm, based on maximum likelihood, for the same set is 0.353.

Track-like and shower-like event topologies are characterized by a different spatial evolution inside the detector, hence in Figure 1 the performances are reported separately.

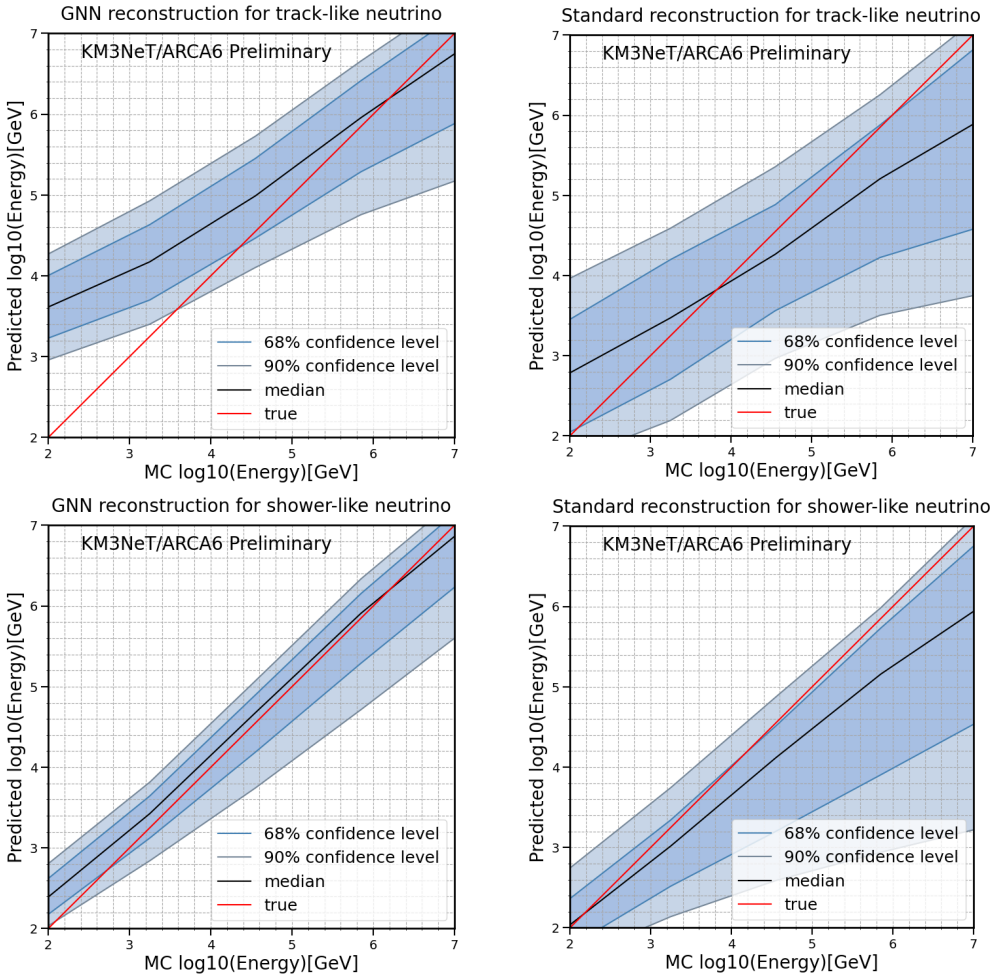

Figure 1: Top: predicted energies versus true MC energies for track-like events in the GNN (*top left*) and standard reconstruction case (*top right*). **Bottom:** predicted energies versus true MC energies for shower-like events in the GNN (*top left*) and standard reconstruction case (*top right*).

It is worth to notice the better performances of the shower-like topologies: in fact the GNN r^2 for shower-like and track-like events is respectively 0.895 and 0.628. This behaviour is probably due to the better event containment for showers.

[1] r^2 is calculated by using the following formula: $r^2 = 1 - \frac{SS_{res}}{SS_{tot}}$ where SS_{res} is the residual sum of squares $\sum_{i=1}^{n}(y_i^{true} - y_i^{pred})^2$ and SS_{tot} is the total sum of squares $\sum_{i=1}^{n}(y_i^{true} - \bar{y}^{true})^2$.

3.2 Neutrino direction regression

The reconstruction of the neutrino direction is performed by a similar GNN as adopted for the energy estimation but followed in this case by three parallel layers, one for each component of the neutrino direction $CosX$, $CosY$, $CosZ$, with custom cosine activation function. The training, validation and test events are the same as in the energy regression case.

In Figure 2 the performances for the reconstruction of the neutrino zenith with the GNN and the standard reconstruction algorithms are reported. The GNN reconstructions show a better behavior compared to the standard method for both the shower-like component ($r^2_{GNN} = 0.74$ vs. $r^2_{STD} = 0.58$) and the track-like component ($r^2_{GNN} = 0.96$ vs. $r^2_{STD} = 0.78$). The track-like component plot for the GNN case exhibits a narrow distribution around the trues values respect the standard reconstruction. However, the median of the distribution produced by the standard reconstruction shows a better agreement with the true values. The other directions show similar behavior, so they will be omitted here.

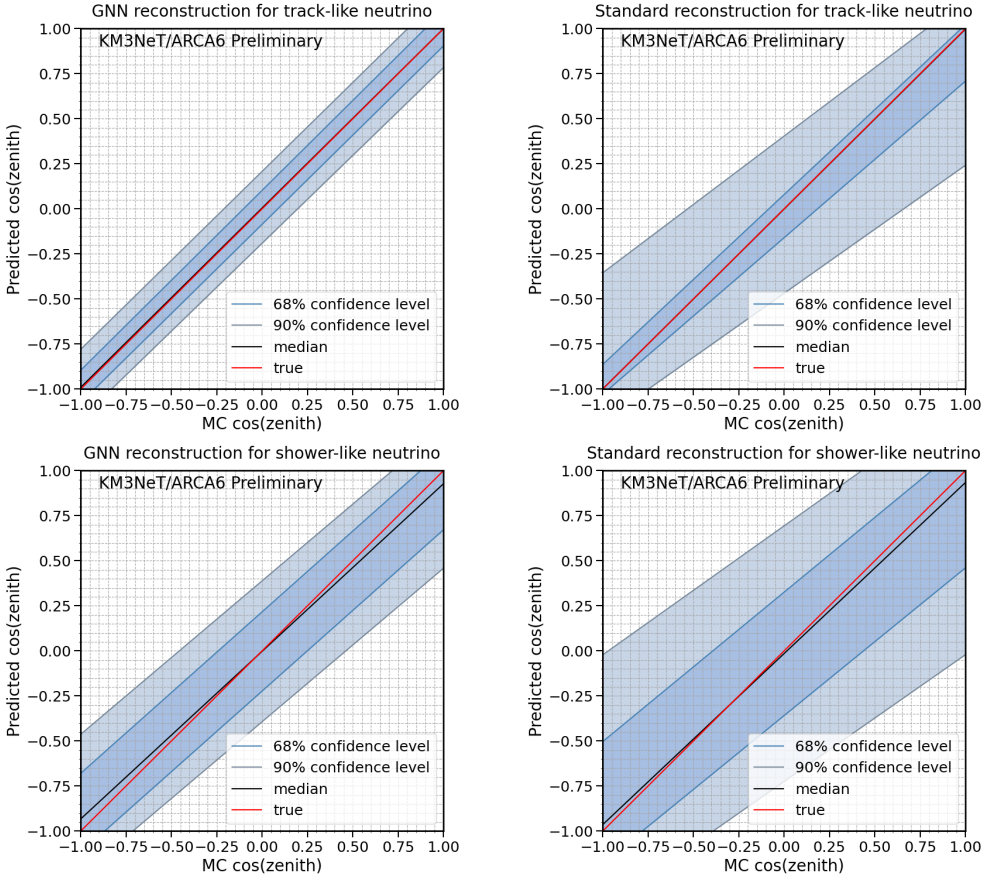

Figure 2: Top: predicted cosine of the zenith versus true MC value for the GNN (*top left*) and the standard reconstruction case (*top right*) for the track-like component. **Bottom:** predicted cosine of the zenith versus true MC for the GNN (*bottom left*) and standard reconstruction case (*bottom right*) for the shower component.

The trained models have also been used for inference on real data: Figure 3 shows the data to Monte Carlo comparison for energy and zenith regression.

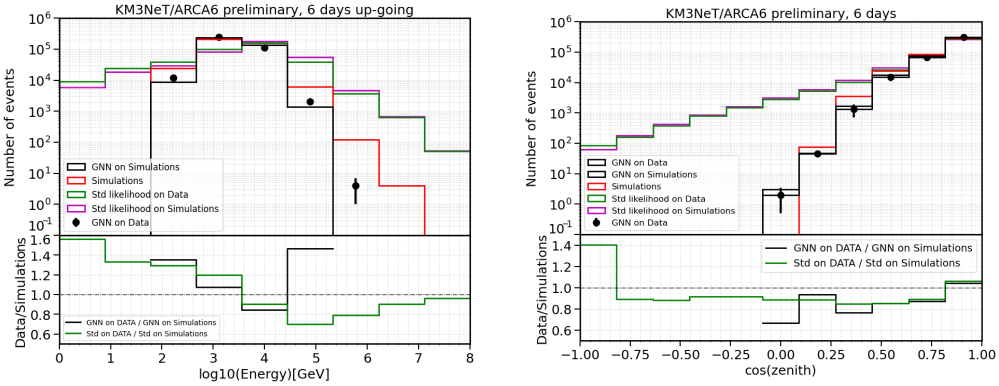

Figure 3: Comparisons of the inferred energies (left) and cos(zenith) (right), varying the inference test data set and reconstruction methods.

The previous plots have been obtained applying a cut on the number of triggered hits for each event in order to suppress events generated by environmental optical background, mainly due to ^{40}K decay. The good agreement between the GNN inference on real data (back dots), GNN inference on Monte Carlo (black lines), and the Monte Carlo simulated value (red lines) for both energy and zenith is clearly noticeable.

4. Signal/background classification

A classification model has been trained to distinguish between atmospheric muons and neutrinos. The classifier produces a score for each event, ranging from 0 to 1, that represents the probability of the event to be of a certain class. During the training phase the GNN takes as input graphs created from MC simulations of the recorded hits for each event: specifically, each hit represents a node of the graph and causality relations between hits represent the edges of the graph. The training process exploits approximately 90% of the data set for training and 10% for validation. Three training sessions were conducted, one for each different detector configuration geometry: one for ARCA with 6 active DUs (ARCA6), one using ARCA7 and one employing ARCA8. The training sets consist of 800k events for ARCA6, 500k for ARCA7, and 1 million events for ARCA8, all with a fraction of 50% atmospheric muons and 50% neutrinos. The networks are trained with k-nearest neighbors equal to $k = 16$, ReLU activation function and Adam optimizer ($\beta_1 = 0.9$, $\beta_2 = 0.999$ and $\varepsilon = 0.1$).
The inference of the network trained on ARCA6 has been performed on a total lifetime of 45 days, for the ARCA7 trained GNN, a period of 25.5 days has been used, while for the network trained on ARCA8, a period of 22.2 days was examined. In total 93 days have been analysed. The analysis results are depicted in Figure 4, where the probability for each event to be classified as neutrino is reported. In order to exclude events mainly due to ^{40}K decay, the same event selection described in Section 3.2 has been applied. It can be noted a peak of events with very high neutrino score in the data, compatible with an excess of atmospheric neutrinos in that region of the neutrino score. The data-Monte Carlo comparison is compatible with values obtained in other KM3NeT analyses, exploiting other selection methodologies [4].

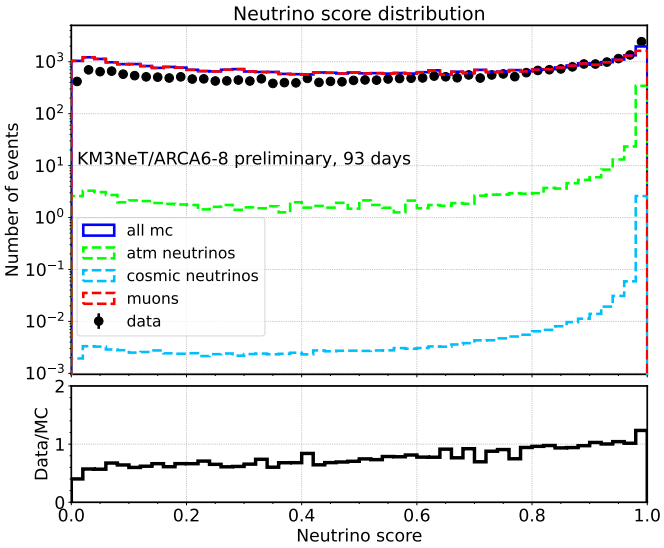

Figure 4: Probability of the events to be classified as neutrino for ARCA6-8.

5. Muon bundles reconstruction

The bulk of events measured in a neutrino telescope corresponds to atmospheric muons, induced by the interaction of cosmic rays (CRs) with the nuclei in the atmosphere. A common technique of background rejection is to use the Earth as a shield, selecting therefore only upgoing particles. Atmospheric muons can be exploited for a variety of physics cases and detector checks, like primary CR composition studies and validation of detector performances and calibrations. A great challenge is the reconstruction of the properties of atmospheric muons, especially if multiple muons traverse the detector simultaneously (muon bundles) [5].

5.1 Direction reconstruction

A regression model has been trained on Monte Carlo events, in order to infer the direction (zenith and azimuth) of the incoming bundle. Each muon inside the bundle, even if having slightly different zenith angles, is simulated with a parallel direction, therefore the two targets for the regression are uniquely defined. The architecture adopted for this task follows the ParticleNet structure described in Section 2. The difference is in the output activation function, for which a normal distribution is assumed in order to measure also an uncertainty associated to the reconstruction. In Figure 5, the 2D distribution of predicted cosine of zenith as a function of the true simulated value is reported, after applying a cut on the uncertainty value itself.

The training sample was composed of ∼2 million events, and the validation set was chosen to be 10% of the training one.

An important aspect of Deep Learning algorithms is their robustness, when applied to data. The performance of the GNN algorithm is compared to the standard reconstruction which is based on the maximization of a likelihood function. The data-Monte Carlo comparison for both the algorithms is reported in Figure 6.

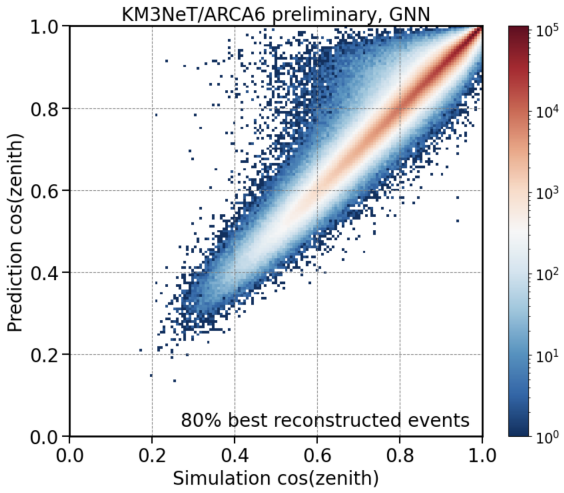

Figure 5: 2D distribution of the predicted cosine of zenith as a function of the true MC one, selecting the best 80% reconstructed events, cutting on the uncertainty estimation.

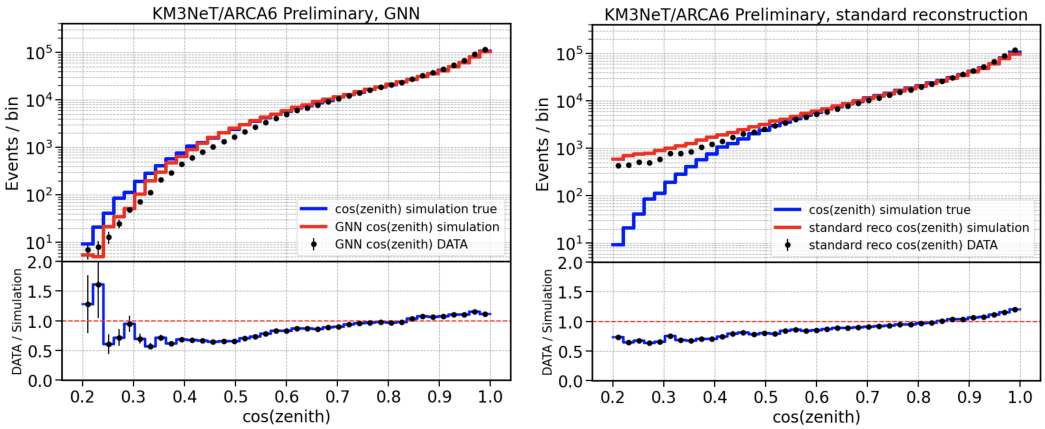

Figure 6: Data-Monte Carlo comparison of the reconstructed cosine of the zenith angle for the GNN (**left**) and for the standard algorithm (**right**). In both plots the Monte Carlo true cosine of the zenith is also reported.

5.2 Muon bundle multiplicity reconstruction

A graph neural network was also trained in order to infer the number of muons in a bundle traversing simultaneously the detector, called *muon multiplicity*. The muon multiplicity is a very important parameter since it allows various studies of CRs and their interactions, and in particular to estimate the mass of the CR primary particle. At the same time, the light yield produced by muon bundles, when traversing the detector, is collected and reconstructed by classical algorithms as a single muon, with energy equal to the sum of the energies of the muons in the bundle.

The choice on the architecture was done similarly to the direction regression task, even if the muon multiplicity is a discrete quantity, and bound from below. An example of the network capabilities is shown in Figure 7: the 2D histogram represents the predicted multiplicity in function of the true one. Also in this case the network is capable to provide not only the inferred multiplicity on a given event but also the error on the estimate itself. In Figure 7 also the data-Monte Carlo

comparison for the predicted muon multiplicity is reported showing a general agreement, especially at mid to high muon multiplicities.

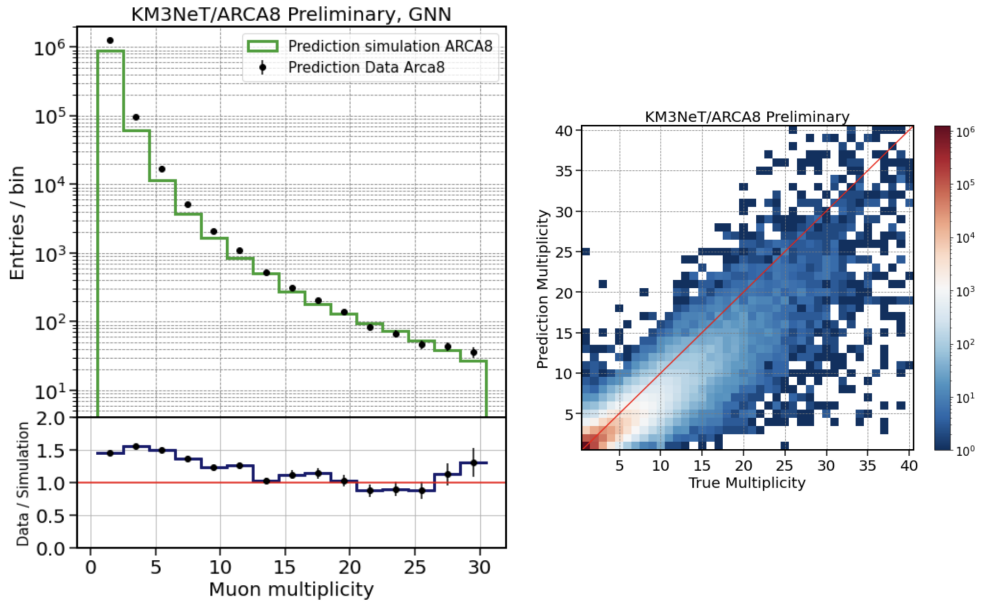

Figure 7: Left: Data Monte Carlo comparison on ARCA8 data set for GNN predicted muon multiplicity. **Right:** 2D histogram showing the predicted muon multiplicity in function of the true one for ARCA8 data set.

Acknowledgments

A. Domi acknowledges the support by the HORIZON-MSCA-2021-PF-01 project QGRANT No. 101068013.

References

[1] KM3NeT collaboration, *Letter of intent for KM3NeT 2.0*, *J. Phys. G* **43** (2016) 084001 [1601.07459].

[2] KM3NeT collaboration, *Event reconstruction for KM3NeT/ORCA using convolutional neural networks*, *JINST* **15** (2020) P10005 [2004.08254].

[3] H. Qu and L. Gouskos, *ParticleNet: Jet Tagging via Particle Clouds*, *Phys. Rev. D* **101** (2020) 056019 [1902.08570].

[4] KM3NeT collaboration, *Search for a diffuse astrophysical neutrino flux using ARCA data*, *PoS* **ICRC2023** (these proceedings) 1195.

[5] KM3NeT collaboration, *Muon bundle reconstruction with KM3NeT/ORCA using graph convolutional networks*, *PoS* **ICRC2021** (2021) 1048.

Full Authors List: The KM3NeT Collaboration

S. Aiello[a], A. Albert[b,bd], S. Alves Garre[c], Z. Aly[d], A. Ambrosone[f,e], F. Ameli[g], M. Andre[h], E. Androutsou[i], M. Anguita[j], L. Aphecetche[k], M. Ardid[l], S. Ardid[l], H. Atmani[m], J. Aublin[n], L. Bailly-Salins[o], Z. Bardačová[q,p], B. Baret[n], A. Bariego-Quintana[c], S. Basegmez du Pree[r], Y. Becherini[n], M. Bendahman[m,n], F. Benfenati[t,s], M. Benhassi[u,e], D. M. Benoit[v], E. Berbee[r], V. Bertin[d], S. Biagi[w], M. Boettcher[x], D. Bonanno[w], J. Boumaaza[m], M. Bouta[y], M. Bouwhuis[r], C. Bozza[z,e], R. M. Bozza[f,e], H.Brânzaş[aa], F. Bretaudeau[k], R. Bruijn[ab,r], J. Brunner[d], R. Bruno[a], E. Buis[ac,r], R. Buompane[u,e], J. Busto[d], B. Caiffi[ad], D. Calvo[c], S. Campion[g,ae], A. Capone[g,ae], F. Carenini[t,s], V. Carretero[c], T. Cartraud[n], P. Castaldi[af,s], V. Cecchini[c], S. Celli[g,ae], L. Cerisy[d], M. Chabab[ag], M. Chadolias[ah], A. Chen[ai], S. Cherubini[aj,w], T. Chiarusi[s], M. Circella[ak], R. Cocimano[w], J. A. B. Coelho[n], A. Coleiro[n], R. Coniglione[w] P. Coyle[d], A. Creusot[n], A. Cruz[al], G. Cuttone[w], R. Dallier[k], Y. Darras[ah], A. De Benedittis[e], B. De Martino[d], V. Decoene[k], R. Del Burgo[e], U. M. Di Cerbo[e], L. S. Di Mauro[w], I. Di Palma[g,ae], A. F. Díaz[j], C. Diaz[j], D. Diego-Tortosa[w], C. Distefano[w], A. Domi[ah], C. Donzaud[n], D. Dornic[d], M. Dörr[am], E. Drakopoulou[i], D. Drouhin[b,bd], R. Dvornický[q], T. Eberl[ah], E. Eckerová[q,p], A. Eddymaoui[m], T. van Eeden[r], M. Eff[n], D. van Eijk[r], I. El Bojaddaini[y], S. El Hedri[n], A. Enzenhöfer[d], G. Ferrara[w], M. D. Filipović[an], F. Filippini[t,s], D. Franciotti[w], L. A. Fusco[z,e], J. Gabriel[ao], S. Gagliardini[g], T. Gal[ah], J. García Méndez[l], A. Garcia Soto[c], C. Gatius Oliver[r], N. Geißelbrecht[ah], H. Ghaddari[y], L. Gialanella[e,u], B. K. Gibson[v], E. Giorgio[w], I. Goos[n], D. Goupilliere[o], S. R. Gozzini[c], R. Gracia[ah], K. Graf[ah], C. Guidi[ap,ad], B. Guillon[o], M. Gutiérrez[aq], H. van Haren[ar], A. Heijboer[r], A. Hekalo[am], L. Hennig[ah], J. J. Hernández-Rey[c], F. Huang[d], W. Idrissi Ibnsalih[e], G. Illuminati[s], C. W. James[al], M. de Jong[as,r], P. de Jong[ab,r], B. J. Jung[r], P. Kalaczyński[at,be], O. Kalekin[ah], U. F. Katz[ah], N. R. Khan Chowdhury[c], A. Khatun[q], G. Kistauri[av,au], C. Kopper[ah], A. Kouchner[aw,n], V. Kulikovskiy[ad], R. Kvatadze[av], M. Labalme[o], R. Lahmann[ah], G. Larosa[w], C. Lastoria[d], A. Lazo[c], S. Le Stum[d], G. Lehaut[o], E. Leonora[a], N. Lessing[c], G. Levi[t,s], M. Lindsey Clark[n], F. Longhitano[a], J. Majumdar[r], L. Malerba[ad], F. Mamedov[p], J. Mańczak[c], A. Manfreda[e], M. Marconi[ap,ad], A. Margiotta[t,s], A. Marinelli[e,f], C. Markou[i], L. Martin[k], J. A. Martínez-Mora[l], F. Marzaioli[u,e], M. Mastrodicasa[ae,g], S. Mastroianni[e], S. Miccichè[w], G. Miele[f,e], P. Migliozzi[e], E. Migneco[w], M. L. Mitsou[e], C. M. Mollo[e], L. Morales-Gallegos[u,e], C. Morley-Wong[al], A. Moussa[y], I. Mozun Mateo[ay,ax], R. Muller[r], M. R. Musone[e,u], M. Musumeci[w], L. Nauta[r], S. Navas[aq], A. Nayerhoda[ak], C. A. Nicolau[g], B. Nkosi[ai], B. Ó Fearraigh[ab,r], V. Oliviero[f,e], A. Orlando[w], E. Oukacha[n], D. Paesani[w], J. Palacios González[c], G. Papalashvili[au], V. Parisi[ap,ad], E.J. Pastor Gomez[c], A. M. Păun[aa], G. E. Păvălaş[aa], S. Peña Martínez[n], M. Perrin-Terrin[d], J. Perronnel[o], V. Pestel[ay], R. Pestes[n], P. Piattelli[w], C. Poirè[z,e], V. Popa[aa], T. Pradier[b], S. Pulvirenti[w], G. Quéméner[o], C. Quiroz[l], U. Rahaman[c], N. Randazzo[a], R. Randriatoamanana[k], S. Razzaque[az], I. C. Rea[e], D. Real[c], S. Reck[ah], G. Riccobene[w], J. Robinson[x], A. Romanov[ap,ad], A. Šaina[c], F. Salesa Greus[c], D. F. E. Samtleben[as,r], A. Sánchez Losa[c,ak], S. Sanfilippo[w], M. Sanguineti[ap,ad], C. Santonastaso[ba,e], D. Santonocito[w], P. Sapienza[w], J. Schnabel[ah], J. Schumann[ah], H. M. Schutte[x], J. Seneca[r], N. Sennan[y], B. Setter[ah], I. Sgura[ak], R. Shanidze[au], Y. Shitov[p], F. Šimkovic[q], A. Simonelli[e], A. Sinopoulou[a], M.V. Smirnov[ah], B. Spisso[e], M. Spurio[t,s], D. Stavropoulos[i], I. Štekl[p], M. Taiuti[ap,ad], Y. Tayalati[m], H. Tedjditi[ad], H. Thiersen[x], I. Tosta e Melo[a,aj], B. Trocmé[n], V. Tsourapis[i], E. Tzamariudaki[i], A. Vacheret[o], V. Valsecchi[w], V. Van Elewyck[aw,n], G. Vannoye[d], G. Vasileiadis[bb], F. Vazquez de Sola[r], C. Verilhac[n], A. Veutro[g,ae], S. Viola[w], D. Vivolo[u,e], J. Wilms[bc], E. de Wolf[ab,r], H. Yepes-Ramirez[l], G. Zarpapis[i], S. Zavatarelli[ad], A. Zegarelli[g,ae], D. Zito[w], J. D. Zornoza[c], J. Zúñiga[c], and N. Zywucka[x].

[a] INFN, Sezione di Catania, Via Santa Sofia 64, Catania, 95123 Italy
[b] Université de Strasbourg, CNRS, IPHC UMR 7178, F-67000 Strasbourg, France
[c] IFIC - Instituto de Física Corpuscular (CSIC - Universitat de València), c/Catedrático José Beltrán, 2, 46980 Paterna, Valencia, Spain
[d] Aix Marseille Univ, CNRS/IN2P3, CPPM, Marseille, France
[e] INFN, Sezione di Napoli, Complesso Universitario di Monte S. Angelo, Via Cintia ed. G, Napoli, 80126 Italy
[f] Università di Napoli "Federico II", Dip. Scienze Fisiche "E. Pancini", Complesso Universitario di Monte S. Angelo, Via Cintia ed. G, Napoli, 80126 Italy
[g] INFN, Sezione di Roma, Piazzale Aldo Moro 2, Roma, 00185 Italy
[h] Universitat Politècnica de Catalunya, Laboratori d'Aplicacions Bioacústiques, Centre Tecnològic de Vilanova i la Geltrú, Avda. Rambla Exposició, s/n, Vilanova i la Geltrú, 08800 Spain
[i] NCSR Demokritos, Institute of Nuclear and Particle Physics, Ag. Paraskevi Attikis, Athens, 15310 Greece
[j] University of Granada, Dept. of Computer Architecture and Technology/CITIC, 18071 Granada, Spain
[k] Subatech, IMT Atlantique, IN2P3-CNRS, Université de Nantes, 4 rue Alfred Kastler - La Chantrerie, Nantes, BP 20722 44307 France
[l] Universitat Politècnica de València, Instituto de Investigación para la Gestión Integrada de las Zonas Costeras, C/ Paranimf, 1, Gandia, 46730 Spain
[m] University Mohammed V in Rabat, Faculty of Sciences, 4 av. Ibn Battouta, B.P. 1014, R.P. 10000 Rabat, Morocco
[n] Université Paris Cité, CNRS, Astroparticule et Cosmologie, F-75013 Paris, France
[o] LPC CAEN, Normandie Univ, ENSICAEN, UNICAEN, CNRS/IN2P3, 6 boulevard Maréchal Juin, Caen, 14050 France
[p] Czech Technical University in Prague, Institute of Experimental and Applied Physics, Husova 240/5, Prague, 110 00 Czech Republic
[q] Comenius University in Bratislava, Department of Nuclear Physics and Biophysics, Mlynska dolina F1, Bratislava, 842 48 Slovak Republic
[r] Nikhef, National Institute for Subatomic Physics, PO Box 41882, Amsterdam, 1009 DB Netherlands
[s] INFN, Sezione di Bologna, v.le C. Berti-Pichat, 6/2, Bologna, 40127 Italy
[t] Università di Bologna, Dipartimento di Fisica e Astronomia, v.le C. Berti-Pichat, 6/2, Bologna, 40127 Italy
[u] Università degli Studi della Campania "Luigi Vanvitelli", Dipartimento di Matematica e Fisica, viale Lincoln 5, Caserta, 81100 Italy
[v] E. A. Milne Centre for Astrophysics, University of Hull, Hull, HU6 7RX, United Kingdom

[w] INFN, Laboratori Nazionali del Sud, Via S. Sofia 62, Catania, 95123 Italy
[x] North-West University, Centre for Space Research, Private Bag X6001, Potchefstroom, 2520 South Africa
[y] University Mohammed I, Faculty of Sciences, BV Mohammed VI, B.P. 717, R.P. 60000 Oujda, Morocco
[z] Università di Salerno e INFN Gruppo Collegato di Salerno, Dipartimento di Fisica, Via Giovanni Paolo II 132, Fisciano, 84084 Italy
[aa] ISS, Atomistilor 409, Măgurele, RO-077125 Romania
[ab] University of Amsterdam, Institute of Physics/IHEF, PO Box 94216, Amsterdam, 1090 GE Netherlands
[ac] TNO, Technical Sciences, PO Box 155, Delft, 2600 AD Netherlands
[ad] INFN, Sezione di Genova, Via Dodecaneso 33, Genova, 16146 Italy
[ae] Università La Sapienza, Dipartimento di Fisica, Piazzale Aldo Moro 2, Roma, 00185 Italy
[af] Università di Bologna, Dipartimento di Ingegneria dell'Energia Elettrica e dell'Informazione "Guglielmo Marconi", Via dell'Università 50, Cesena, 47521 Italia
[ag] Cadi Ayyad University, Physics Department, Faculty of Science Semlalia, Av. My Abdellah, P.O.B. 2390, Marrakech, 40000 Morocco
[ah] Friedrich-Alexander-Universität Erlangen-Nürnberg (FAU), Erlangen Centre for Astroparticle Physics, Nikolaus-Fiebiger-Straße 2, 91058 Erlangen, Germany
[ai] University of the Witwatersrand, School of Physics, Private Bag 3, Johannesburg, Wits 2050 South Africa
[aj] Università di Catania, Dipartimento di Fisica e Astronomia "Ettore Majorana", Via Santa Sofia 64, Catania, 95123 Italy
[ak] INFN, Sezione di Bari, via Orabona, 4, Bari, 70125 Italy
[al] International Centre for Radio Astronomy Research, Curtin University, Bentley, WA 6102, Australia
[am] University Würzburg, Emil-Fischer-Straße 31, Würzburg, 97074 Germany
[an] Western Sydney University, School of Computing, Engineering and Mathematics, Locked Bag 1797, Penrith, NSW 2751 Australia
[ao] IN2P3, LPC, Campus des Cézeaux 24, avenue des Landais BP 80026, Aubière Cedex, 63171 France
[ap] Università di Genova, Via Dodecaneso 33, Genova, 16146 Italy
[aq] University of Granada, Dpto. de Física Teórica y del Cosmos & C.A.F.P.E., 18071 Granada, Spain
[ar] NIOZ (Royal Netherlands Institute for Sea Research), PO Box 59, Den Burg, Texel, 1790 AB, the Netherlands
[as] Leiden University, Leiden Institute of Physics, PO Box 9504, Leiden, 2300 RA Netherlands
[at] National Centre for Nuclear Research, 02-093 Warsaw, Poland
[au] Tbilisi State University, Department of Physics, 3, Chavchavadze Ave., Tbilisi, 0179 Georgia
[av] The University of Georgia, Institute of Physics, Kostava str. 77, Tbilisi, 0171 Georgia
[aw] Institut Universitaire de France, 1 rue Descartes, Paris, 75005 France
[ax] IN2P3, 3, Rue Michel-Ange, Paris 16, 75794 France
[ay] LPC, Campus des Cézeaux 24, avenue des Landais BP 80026, Aubière Cedex, 63171 France
[az] University of Johannesburg, Department Physics, PO Box 524, Auckland Park, 2006 South Africa
[ba] Università degli Studi della Campania "Luigi Vanvitelli", CAPACITY, Laboratorio CIRCE - Dip. Di Matematica e Fisica - Viale Carlo III di Borbone 153, San Nicola La Strada, 81020 Italy
[bb] Laboratoire Univers et Particules de Montpellier, Place Eugène Bataillon - CC 72, Montpellier Cédex 05, 34095 France
[bc] Friedrich-Alexander-Universität Erlangen-Nürnberg (FAU), Remeis Sternwarte, Sternwartstraße 7, 96049 Bamberg, Germany
[bd] Université de Haute Alsace, rue des Frères Lumière, 68093 Mulhouse Cedex, France
[be] AstroCeNT, Nicolaus Copernicus Astronomical Center, Polish Academy of Sciences, Rektorska 4, Warsaw, 00-614 Poland

Acknowledgements

The authors acknowledge the financial support of the funding agencies: Agence Nationale de la Recherche (contract ANR-15-CE31-0020), Centre National de la Recherche Scientifique (CNRS), Commission Européenne (FEDER fund and Marie Curie Program), LabEx UnivEarthS (ANR-10-LABX-0023 and ANR-18-IDEX-0001), Paris Île-de-France Region, France; Shota Rustaveli National Science Foundation of Georgia (SRNSFG, FR-22-13708), Georgia; The General Secretariat of Research and Innovation (GSRI), Greece Istituto Nazionale di Fisica Nucleare (INFN), Ministero dell'Università e della Ricerca (MIUR), PRIN 2017 program (Grant NAT-NET 2017W4HA7S) Italy; Ministry of Higher Education, Scientific Research and Innovation, Morocco, and the Arab Fund for Economic and Social Development, Kuwait; Nederlandse organisatie voor Wetenschappelijk Onderzoek (NWO), the Netherlands; The National Science Centre, Poland (2021/41/N/ST2/01177); The grant "AstroCeNT: Particle Astrophysics Science and Technology Centre", carried out within the International Research Agendas programme of the Foundation for Polish Science financed by the European Union under the European Regional Development Fund; National Authority for Scientific Research (ANCS), Romania; Grants PID2021-124591NB-C41, -C42, -C43 funded by MCIN/AEI/ 10.13039/501100011033 and, as appropriate, by "ERDF A way of making Europe", by the "European Union" or by the "European Union NextGenerationEU/PRTR", Programa de Planes Complementarios I+D+I (refs. ASFAE/2022/023, ASFAE/2022/014), Programa Prometeo (PROMETEO/2020/019) and GenT (refs. CIDEGENT/2018/034, /2019/043, /2020/049. /2021/23) of the Generalitat Valenciana, Junta de Andalucía (ref. SOMM17/6104/UGR, P18-FR-5057), EU: MSC program (ref. 101025085), Programa María Zambrano (Spanish Ministry of Universities, funded by the European Union, NextGenerationEU), Spain; The European Union's Horizon 2020 Research and Innovation Programme (ChETEC-INFRA - Project no. 101008324).